表1　小児の人工内耳入れ替え症例の詳細

	初回手術				入れ替え手術			
症例	失聴原因	術側	年齢(歳) 性別	・機種 ・挿入アクティブ電極数	原因	初回手術からの期間(月)	・機種 ・挿入アクティブ電極数	手術所見
1	先天性	左	5 男	・CI22M ・全電極	Soft failure	73	・CI24M ・全電極	挿入スムーズ
2	コモンキャビティー	左	3 女	・CI22M ・21個	Hard failure	72	・CI24M ・16個	挿入スムーズ
3	両側進行性感音難聴	左	11 女	・CI24M ・全電極	電極の変位	85	・HiRes 90K (Hifocus 1j) ・全電極	挿入スムーズ
4	両側進行性感音難聴	左	11 女	・CI24M ・全電極	Hard failure	22	・CI24M ・全電極	挿入スムーズ
5	先天性	右	2 女	・CI24M ・全電極	感染 機器本体の皮膚露出	39	・HiRes 90K (Hifocus 1j) ・全電極	挿入スムーズ
6	ムンプス	右	5 女	・CI24R（CS） ・全電極	感染 機器本体の皮膚露出	11	・CI24R（CS） ・全電極	挿入スムーズ

表2　成人の人工内耳入れ替え症例の詳細

	初回手術				入れ替え手術			
症例	失聴原因	術側	年齢(歳) 性別	・機種 ・挿入アクティブ電極数	原因	初回手術からの期間(月)	・機種 ・挿入アクティブ電極数	手術所見
7	両側進行性感音難聴	右	60 男	・CI22M ・全電極	Soft failure	30	・Clarion 1，2 ・全電極	挿入スムーズ
8	左突発性難聴 右慢性中耳炎	左	55 男	・CI22M ・全電極	Soft failure	139	・CI24M ・全電極	挿入スムーズ
9	左真珠腫性中耳炎 右慢性中耳炎	右	49 男	・CI22M ・全電極	Soft failure	127	・CI24M ・12個	蝸牛内閉塞にて 挿入困難
10	両側慢性中耳炎	右	55 男	・CI22M ・全電極	電極の変位	60	・CI24M ・全電極	蝸牛内閉塞にて 挿入困難

になるように提示）で，回答は口頭あるいは書字にて求め，正答率を算出した．対象症例における母音，子音，文節の術前後聴取能の成績を Wilcoxon の符号付き順位検定を用いて比較検討した．

結　　果

電極の入れ替えを要した手術症例は10名であり，その内訳は小児６名，成人４例であった．このうち他院で初回の人工内耳手術を施行されていた症例は小児，成人でそれぞれ１名であり，当院での入れ替えの割合は全体で3.2%，小児で3.9%，成人で2.4%であった．全症例で初回手術と同側に電極の再挿入が施行された．

対象症例の詳細を小児，成人に分けて表１，２に示した．

初回手術から入れ替え手術までの期間は小児で11カ月から85カ月（平均50.3カ月），成人で30カ月から139カ月

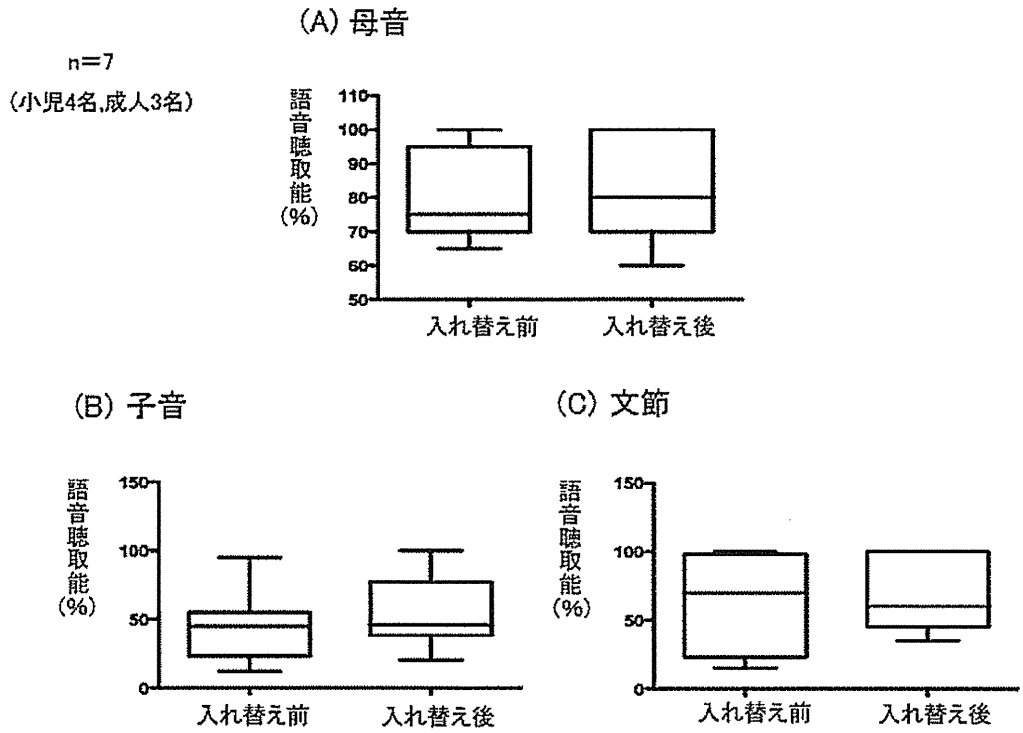

図1　人工内耳入れ替え症例の入れ替え前後の母音（A），子音（B），文節（C）における語音聴取能の成績

（平均89カ月）であった．初回電極を摘出し，間隔をおいて電極の再挿入を施行した症例は3名（症例5，6，8）であった．

入れ替えの最多の原因として小児ではHard failureと，感染と人工内耳機器本体の皮膚への露出がそれぞれ2名（小児全体の33%），成人ではSoft failureが3名（成人全体の75%）であった．

初回機種として全症例でコクレア社のCI22M，CI24MもしくはCI24R（CS）を使用していた．入れ替え機種として初回と同じ機種もしくは上位機種を選択した症例は7名であった．CI24MからHiRes 90K（電極はHifocus 1j）へ変更した症例は2名，CI22MからClarion1，2へ変更した症例は1名であった．

電極の再挿入に関して全アクティブ電極を埋め込むことができた症例は8名（80%）であった．全アクティブ電極を埋め込むことができた症例のうち1例と，部分的埋め込みに終わった2例のうち1例で，蝸牛内に肉芽増生を認めた．

電極入れ替え前後の語音聴取能を比較できた症例は7名（小児4名，成人3名）であった．母音，子音，文節における術前後の語音聴取能の結果を図1(A)，(B)，(C)に示す．いずれも統計学的に有意な差を認めなかった（p＝母音：0.78，子音：0.31，文節：0.69，Wilcoxonの符号付き順位検定）．

考　　察

人工内耳手術における入れ替え手術症例の割合は5.1～6.7%と報告されている[2)5)6)7)]．当科での人工内耳入れ替え手術症例の割合は全体で3.2%と他の報告よりも頻度が低かった．入れ替えの原因としてBalkanyら[9)]はDevice failureを分類に挙げている．その後Device failureはhard failureとsoft failureに分類されている[8)]．Hard failureの定義は語音聴取能の低下を伴い，インテグリティーテストで異常がある場合，Soft failureの定義は語音聴取能の低下や耳鳴りなどの聴覚的症状，痛みや顔面神経痙攣などの非聴覚的症状を随伴し，インテグリティーテストで異常なしとされた場合とされている．つまりHard failureが機器の明らかな物理的故障であるの対して，Soft failureは電極の変位などの異常がないにもかかわらずパーフォマンスの低下を認め，機器の異常が疑わしい状態と解釈できる．電極入れ替えの原因としてBalkanyら[2)]，はDevice failureが最多であったと報告している．その中でもHard failureが原因として多かったとする報告[5)7)]もみられる一方で，Buchmanら[10)]は成人ではSoft failureが多かったとも報告している．また小児では頭部外傷による機器の故障が多いとの報告もある[6)]．今回症例4，5は頭部外傷が契機で電極の入れ替えを必要としており，小児において頭部外傷は入れ替えの原因の重要な要素の一因と思われる．感染と機器本体

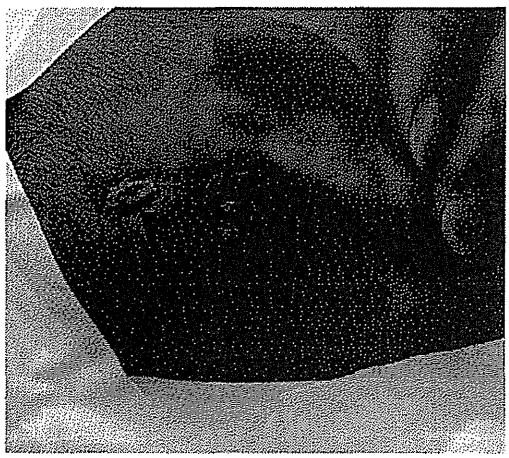

図2　症例5における右耳後部所見．
当初は点線矢印部に滲出液貯留を認め，次第に機種本体の突出を認めるようになった（実線矢印部）．

図3　症例6における右耳後部所見．
炎症部位の周囲に一部肉芽形成を認める（矢印部）．

の皮膚への露出が原因となり，入れ替えを行った症例は症例5，6の小児における症例であった．症例5は頭部外傷を契機に機器本体がある皮膚直下に滲出液の貯留を認めるようになり，外来で同部位を穿刺排液し同部位を圧迫しながら経過観察していた．滲出液の培養検査では起因菌は検出されなかったが，次第に機器本体の皮膚への露出を認めるようになった（図2）．症例6は術後しばらくしてから機器本体周囲に発赤と圧痛を伴うようになり，同部位から膿汁を認めるようになった．培養からはMRSAが検出されたため，同部位を消毒処置しながらバンコマイシンの点滴を施行したが炎症部位周囲に肉芽が形成され，症状の改善を認めなかった（図3）．いずれの症例でも当初は抗生剤の点滴や炎症周囲の消毒などを施行するも，次第に増悪傾向をたどり機器本体の抜去を余儀なくされた．感染により電極を摘出した小児の全例において蝸牛内に電極を留置したまま人工内耳機器本体を摘出して，感染兆候が消失してから再挿入術を施行した．このように蝸牛内に初回電極を留置しておくことで，電極の再挿入はスムーズに行うことができた．また機器本体の抜去時に肉芽をできるだけ除去する，入れ替え時に機器本体を容れる骨溝を初回に作成した位置からややずらすといった工夫を再発防止目的に施行した．Kundaら[11]は炎症により機器本体が露出したにもかかわらず起因菌が検出されず，人工内耳機器に使用されているシリコンアレルギーが原因であった症例を報告している．症例6ではCI24R（CS）で使用されているすべてのシリコンに対して皮膚科主導でパッチテストを施行したが，すべて陰性であった．その後皮膚科でパッチテストキットの使用を受諾してもらえなくなったため，症例5ではパッチテストを行うことができなかった．シリコンアレルギーが否定できなかったため再手術の際には機種変更を行った．炎症があるにもかかわらず滲出液などから起因菌が検出されず，初回手術から時間の経過を認める症例ではシリコンアレルギーの可能性も考慮する必要がある．また症例3，10は電極の変位が原因となり，入れ替えを行った．症例3は11歳時に左人工内耳埋め込み術を施行し，術後人工内耳の使用は問題なく行えていた．17歳頃よりめまい感，頭痛を訴えるようになり，時間経過とともに語音聴取能の低下，音刺激による気分不快感を認めるようになった．X線写真では電極のスリップアウトを認めたが（図4A），インピーダンス異常高値などから電極の故障の可能性も否定できず人工内耳入れ替え術を行った．術中の所見では電極の一部は蝸牛内からスリップアウトしており，術前の画像所見と一致した．この症例ではアクティブ電極をすべて挿入することができた（図4B）．症例10は内藤ら[12]により報告されているが，慢性中耳炎が背景として存在し左中耳根本術と左人工内耳埋め込み術を施行されていた．乳突部は側頭筋弁を利用して電極を被覆したが，次第に外耳道後壁の陥凹に伴い側頭筋弁の萎縮を認めた．それに伴い一部電極の変位と感染を認め，語音聴取の低下を認めるようになった．

入れ替えに際して聞き取りに対する慣れなどの点を考慮すると初回と同じ音声コード化法をもつ機種を選択した方が好ましいが，今回3例でコクレア社からAdvanced Bionics社（以下AB社）への機種変更を施行した．われわれは入れ替えの際に本邦で使用できるコクレア社，AB社，メドエル社の機種それぞれの特徴の説明を行い，患者の希望と画像などの所見を合わせて機種

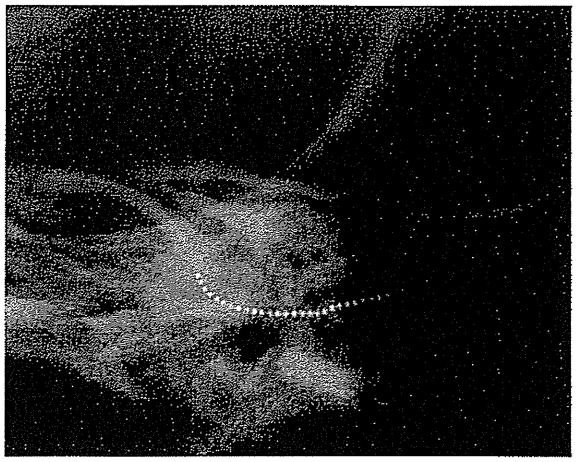

図４Ａ　症例３における電極入れ替え前のＸ線写真．電極のスリップアウトを認める．

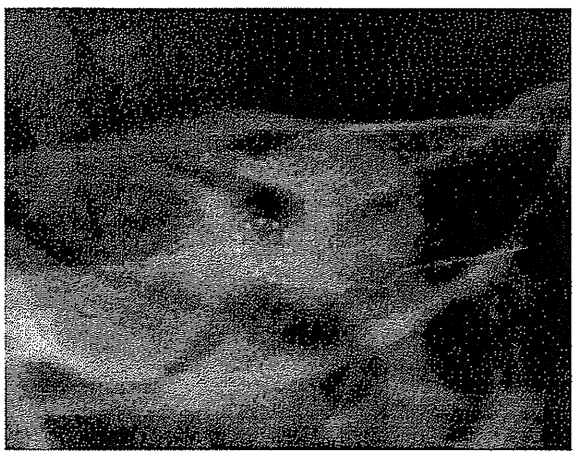

図４Ｂ　症例３における電極入れ替え後のＸ線写真．電極は蝸牛内で１回転半している．

選択を行っている．症例３，５では患者が音楽の聴取に優れた機種を希望し，さらに症例５ではアレルギー反応の可能性も考慮したためAB社を選択した．症例７はコクレア社の人工内耳の使用に伴い顔面痙攣を認めた．顔面痙攣を来す電極の位置から，電極刺激が蝸牛外側壁に及び，外側壁と隣接する顔面神経迷路部が刺激されていると考えた．当時国内で唯一使用可能な蝸牛軸巻き付き型で，蝸牛軸側にのみ電極があるClarion1，２を選択し，術後顔面痙攣は認めなくなった．

電極の再挿入においては術前と同じ電極数の挿入が可能と報告されており[2)5)7)]，今回われわれの報告でも同様であった．今回の報告ではほとんどの症例で前回の蝸牛開窓部をやや広げ，周囲の肉芽を取り除くのみで電極の再挿入はスムーズであった．症例２はコモンキャビティー型[13)]の内耳奇形を認め，初回手術では電極を無理に折り曲げることによって21個の電極を挿入していた．入れ替え手術では電極を無理に屈曲させないようにしたため，初回手術より挿入できた電極数は少なかったが，最終的に使用できている電極数は減っていない．しかし今回われわれは再挿入に難渋した症例を２名経験した．症例10は全電極の再挿入が可能であったものの蝸牛内の肉芽増生により再挿入に難渋し，入れ替え手術を２回施行している症例であり，症例９も蝸牛内の肉芽と骨増生が強く，全電極を挿入することはできなかった．これらの症例を考慮すると，再挿入における電極の選択は重要なポイントとなる．再挿入において初回電極の直径と同等もしくはそれより小さい電極，ストレート電極を選択すべきであるとの報告もある[7)]．今回ほとんどの症例で前回と同様の電極を使用しており，症例６を除いてすべてストレート電極であった．再挿入時にどの電極を使用した方がよいかは症例各々で異なってくるが，それぞれの電極の直径と電極のタイプを理解しておくことは重要と考える．また電極の摘出術と再挿入術を同時に施行しない場合は，初回の電極のみを蝸牛内に残して挿入スペースを確保しておくことが肉芽の増生や骨新生防止の観点から望ましいと考える．しかし症例10ではこれらの段階を踏んだにもかかわらず，再挿入に難渋しており，再挿入に難渋した症例９と同じく慢性中耳炎で失聴していた．この２症例はどちらも初回手術時は蝸牛内に肉芽増生は認めず，その後も明らかな感染・炎症は来していなかったが，再手術の際には蝸牛開窓部から蝸牛内腔にかけて肉芽と骨増生が強かった．氷見ら[14)]は中耳の炎症が正円窓を介して内耳に波及し，鼓室階の基底回転を中心に反応性線維化・骨化を惹起すると報告しており，何らかの形で中耳の炎症が再手術の際の蝸牛内肉芽増生に関係している可能性がある．慢性中耳炎が存在する側の人工内耳の電極入れ替えの際には将来的に電極が露出しないよう工夫することと再挿入に難渋する可能性を考慮しなければならない．

内藤ら[15)]は電極の再挿入は機能面で不利益をもたらさなかったと報告しており，事実他の報告でも術前後の語音聴取はほぼ同等もしくはそれ以上とされている[2)5)7)]．今回のわれわれの検討において統計学的に再手術による悪化は認めなかった．

入れ替え前よりも再挿入できた電極数が少なかった症例２，９ではいずれも入れ替え後の語音聴取能は入れ替え前とほぼ同程度となった．症例９では12個のアクティブ電極しか挿入できなかったが，マップ調節では16本の電極が使用可能であった．いずれの症例でも入れ替え後のマップはT/Cレベル測定値に基づいて作成され，入れ替え前のマップを参考とはしなかった．しかし入れ替

えにより語音聴取の低下を認めた症例も経験している．症例3はincomplete partition型[13]の内耳奇形を認め，CI24MからHiRes 90Kへ機種変更した．この症例では術後3カ月目までは言葉の聞き取りに違和感を述べていたが，6カ月目にはほぼ術前と同様の語音聴取能となった．しかし術後1年目の検査で人工内耳マップのダイナミックレンジが狭くなり，語音聴取の増悪も認めた．しかし人工内耳装用閾値の悪化は認めておらず，現在原因を外来にて精査中である．

再挿入に難渋する可能性も考慮して各機種の特徴を十分に理解し電極を選択する，入れ替え後の語音聴取は大半の場合は術前と同程度もしくはそれ以上であるが，中には低下する場合もあることを電極の入れ替えの際には留意する必要がある．

ま と め

1. 当科における人工内耳入れ替え手術症例を検討した．
2. 入れ替え症例では再挿入はスムーズに行えることが多いが，困難な症例もあるため入れ替え機種と電極の選択は重要である．
3. 入れ替え後の語音聴取能は入れ替え前と比べて有意な悪化は認めなかった．

参 考 文 献

1) Miyamoto RT, Svirsky MA, Myres WA, et al: Cochlear implant reimplantation. Am J Otol 1997; 18: S60-61.
2) Balkany TJ, Hodges AV, Gomez-Marin O, et al: Cochlear reimplantation. Laryngoscope 1999; 109: 351-355.
3) Alexiades G, Ronald JT, Fishman AJ, et al: Cochlear reimplantation: Surgical techniques and functional results. Laryngoscope 2001; 111: 1608-1613.
4) Fayad JN, Baino T, Parisier SC: Revision cochlear implant surgery: Causes and outcome. Otolaryngol Head Neck Surg 2004; 131: 429-432.
5) Lassig AA, Zwolan TA, Telian SA: Cochlear implant failures and revision. Otol Neurotol 2005; 26: 624-634.
6) Weise JB, Muller-Deile J, Brasemann G, et al: Impact to the head increases cochlear implant reimplantation rate in children. Auris Nasus Larynx 2005; 32: 339-343.
7) Côté M, Ferron P, Bergeron F, et al: Cochlear reimplantation: causes of failure, outcomes, and audiologic performance. Laryngoscope 2007; 117: 1225-1235.
8) Brown KD, Connell SS, Balkany TJ, et al: Incidence and indications for revision cochlear implant surgery in adults and children. Laryngoscope 2009; 119: 152-157.
9) Balkany TJ, Hodges AV, Buchman CA, et al: Cochlear implant soft failures consensus development conference statement. Otol Neurotol 2005; 26: 815-818.
10) Buchman CA, Higgins CA, Cullen R, et al: Revision cochlear implant surgery in adult patients with suspected device malfunction. Otol Neurotol 2004; 26: 624-634.
11) Kunda LD, Stidham KR, Inserra MM, et al: Silicone Allergy: A new cause for cochlear implant extrusion and its management. Otol Neurotol 2006; 27: 1078-1082.
12) 内藤　泰，伊藤壽一：人工内耳摘出・再手術を要した症例．JOHNS 2001; 17: 1741-1744.
13) Jackler RK, Luxford WM, House WF: Congenital malformations of the inner ear: a classification based on embrygenesis. Laryngoscope 1987; 97: 2-14.
14) 氷見徹夫：慢性中耳炎耳の人工内耳手術．JOHNS 2004; 20: 69-73.
15) 内藤　明：人工内耳再手術例における機能的評価．臨床福祉 2006; 3: 33-39.

(2010年5月24日受稿　2010年12月3日受理)

別刷請求先　〒918-8501 福井市月見2丁目4-1
福井赤十字病院耳鼻咽喉科　石川正昭

Clinical Outcomes Cochlear Reimplantation

Masaaki Ishikawa, M.D., Harukazu Hiraumi, M.D., Ph.D.*, Norio Yamamoto, M.D., Ph.D.*
Tatsunori Sakamoto, M.D., Ph.D.*, Shinichi Kanemaru, M.D., Ph.D.** and Juichi Ito, M.D., Ph.D.*

Department of Otolaryngology-Head and Neck Surgery, Fukui Red Cross Hospital, Fukui
*Department of Otolaryngology-Head and Neck Surgery, Graduate School of Medicine, Kyoto University, Kyoto
**Department of Otolaryngology-Head and Neck Surgery, Kitano Hospital, Osaka

To clarify the clinical features of cochlear reimplantation and surgical changes in auditory performance, we retrospectively reviewed 10 of 252 cochlear implantation surgeries-6 adults and 4 children-among 129 children and 123 adults done between April 1987 and May 2009. Mean duration from initial implantation to reimplantation was 50.3 months in

children and 89 months in adults, most commonly due to hard failure and implant exposure/infection (33%) in children and to hard failure (75%) in adults. The initial device implanted was the Nucleus multichannel implant (CI22M, CI24M, or CI24R). The second implant in 7 was the same or an upgrade of the same manufacturer's device, and in 2 children the HiRes 90K (Hifocus 1j) and in 1 adult the Clarion 1.2.

Full initial and reinsertion succeeded in 8 cases but reinsertion proved difficult in 2 due to severe intracochlear granulation and osteoneogenseis. Auditory performance analyzed in 7 cases was mostly equal to or better than before reimplantation, although differences were not statistically significant. Reinsertion is rarely difficult, but electrode choice is important in preparing for difficult reinsertion. Post reinsertion auditory performance is satisfactory with some exceptions.

Keywords: cochlear implantation, cochlear reimplantation, cause reimplantation, auditory performance

Nippon Jibiinkoka Gakkai Kaiho (Tokyo) 114: 498–504, 2011

 CMES, vol.1, no.1, pp.1-22, 2011

Ab initio Molecular Dynamics of H_2 Dissociative Adsorption on Graphene Surfaces

Kentaro Doi[12], Ikumi Onishi[1] and Satoyuki Kawano[13]

Abstract: Hydrogen technologies are currently one of the most actively researched topics. A lot of researches have tied to enhance their energy conversion efficiencies. In the present study, numerical analyses have been carried out focusing on hydrogen-storage carbon materials which are expected to realize high gravimetric and volumetric capacities. In particular, dissociative adsorption processes of H_2 molecules above graphene surfaces have been investigated by *ab initio* molecular dynamics. The present results indicate that a steric graphene surface plays an important role in enhancing the charge transfer which induces dissociation of H_2 and adsorption of H atoms on the surface. The dissociation energy required for the reaction $H_2 \rightarrow 2H$ above the steric sites is expected to be reduced to 56.2 % of that in vacuum without graphene. Thus, distorted graphenes are an effective hydrogen-storage material, which functions as a catalytic agent.

Keywords: *Ab initio* MD, Grapehene, Hydrogene storage, Dissociative adsorption

1 Introduction

Recently, hydrogen technologies have received considerable interest as a means of producing clean and safe power supplies. However, several problems, such as portability, safety, and cost performance, have to be solved to realize so-called hydrogen economy. Carbon nanomaterials are one of the most promising candidates for hydrogen-storage materials due to their low weight and high cost performance, compared with other metallic alloys [Dillon, Jones, Bekkedahl, Kiang, Bethune, and Heben (1997); Chen, Wu, Lin, and Tan (1999); Elias, Nair, Mohiuddin, Morozov, Blake, Halsall, Ferrari, Boukhvalov, Katsnelson, Geim, and

[1] Department of Mechanical Science and Bioengineering, Graduate School of Engineering Science, Osaka University, Osaka 560-8531, Japan
[2] doi@me.es.osaka-u.ac.jp
[3] kawano@me.es.osaka-u.ac.jp

Novoselov (2009); Berseth, Harter, Zidan, Blomqvist, Araújo, Scheicher, Ahuja, and Jena (2009); Guisineger, Rutter, Crain, First, and Stroscio (2009); Riedl, Coletti, Iwasaki, Zakharov, and Starke (2009); Riedl, Coletti, and Starke (2010); Virojanadara, Yakimova, Zakharov, and Johansson (2010); Virojanadara, Zakharov, Yakimova, and Johansson (2010); Liu, Fan, Liu, Cong, Cheng, and Dresselhaus (1999); Ströbel, Jörissen, Schliermann, Trapp, Schütz, Bohmhammel, Wolf, and Garche (1999); Yang (2000); Gupta and Srivastava (2000, 2001); Hirscher, Becher, Haluska, Dettlaff-Weglikowska, Quintel, Duesberg, Choi, Downes, Hulman, Roth, Stepanek, and Bernier (2001); Chen, Shaw, Bai, Wang, Lund, Lu, and Chung (2001); Nishimiya, Ishigaki, Takikawa, Ikeda, Hibi, Sakakibara, Matsumoto, and Tsutsumi (2002); Xu, Takahashi, Matsuo, Hattori, Kumagai, Ishiyama, Kaneko, and Iijima (2007)]. A few pioneering experimental studies on hydrogen-chargeable carbon materials have been performed [Dillon, Jones, Bekkedahl, Kiang, Bethune, and Heben (1997); Chen, Wu, Lin, and Tan (1999)], and recent reports indicate that graphene is preferable materials for hydrogen storages [Elias, Nair, Mohiuddin, Morozov, Blake, Halsall, Ferrari, Boukhvalov, Katsnelson, Geim, and Novoselov (2009); Berseth, Harter, Zidan, Blomqvist, Araújo, Scheicher, Ahuja, and Jena (2009); Guisineger, Rutter, Crain, First, and Stroscio (2009); Riedl, Coletti, Iwasaki, Zakharov, and Starke (2009); Riedl, Coletti, and Starke (2010); Virojanadara, Yakimova, Zakharov, and Johansson (2010); Virojanadara, Zakharov, Yakimova, and Johansson (2010)]. It is suggested that distorted surfaces and curvatures of carbon materials play a significant role in hydrogen storage technologies [Elias, Nair, Mohiuddin, Morozov, Blake, Halsall, Ferrari, Boukhvalov, Katsnelson, Geim, and Novoselov (2009); Berseth, Harter, Zidan, Blomqvist, Araújo, Scheicher, Ahuja, and Jena (2009)]. In addition, novel properties of graphene layeres fabricated on SiC substrates have also attracted attentions [Berseth, Harter, Zidan, Blomqvist, Araújo, Scheicher, Ahuja, and Jena (2009); Guisineger, Rutter, Crain, First, and Stroscio (2009); Riedl, Coletti, Iwasaki, Zakharov, and Starke (2009); Riedl, Coletti, and Starke (2010); Virojanadara, Yakimova, Zakharov, and Johansson (2010); Virojanadara, Zakharov, Yakimova, and Johansson (2010)]. In those works, it is reported that hydrogen adsorption and desorption properties are expressed at the interface of graphenes and SiC substrates by the peculiar electronic properties. Theoretical investigations have featured interactions between hydrogen species and carbon nanomaterials, such as carbon nanotubes (CNTs) [Tada, Furuya, and Watanabe (2001); Miura, Kasai, Diño, Nakanishi, and Sugimoto (2003); Nakano, Ohta, Yokoe, Doi, and Tachibana (2006); Doi, Nakano, Ohta, and Tachibana (2007); Durgun, Ciraci, and Yildirim (2008); Hanasaki, Nakamura, Yonebayashi, and Kawano (2008); Cheng, Pez, Kern, Kresse, and Hafner (2001)], carbon nanofibers [Chan, Chen, Gong, and Liu (2001); Li, Furuta, Goto, Ohashi, Fujiwara, and Yip (2003); Cheng, Pez, and Cooper (2003)], and graphenes [Jeloacia and Sidis (1999); Arel-

lano, Molina, Rubio, and Alonso (2000); Okamoto and Miyamoto (2001); Sha and Jackson (2001); Patchkovskii, Tse, Yurchenko, Zhechkov, Heine, and Seifert (2005)]. They reported that surface distortions cause carbon networks to change their bonding states. However, most *ab initio* studies are based on static mechanics of H atoms due to the mathematical difficulty and huge computational cost of modeling dynamic processes of H_2 molecules.

In the present study, a technique for dynamic analysis on reaction systems is developed, based on a coupling procedure of *ab initio* methods and molecular dynamics (MD) for parallel computing. Here, *ab initio* MD computations are effectively used to determine a condition which permits dissociative adsorption of H_2 above graphene surface and to find out detailed chemical reaction pathways from various configurations. We particularly focus on the time-dependent dissociative adsorption of H_2 near graphene surfaces with a view to engineering applications. The dynamic behavior of dissociative adsorption of an H_2 molecule can be treated successfully, overcoming a difficulty to simulate chemical reactions by MD procedures. Consequently, it is confirmed that hydrogen adsorption is enhanced above steric sites of graphene surfaces where the dissociation of H–H is simaltaneously activated. Effective catalytic functions in carbon materials are expected to reduce the cost for metallic catalytic agents. The present results are also well confirmed with an experimental observation [Elias, Nair, Mohiuddin, Morozov, Blake, Halsall, Ferrari, Boukhvalov, Katsnelson, Geim, and Novoselov (2009)].

2 Theoretical methods of solution

Figure 1 shows a schematic illustration of our theoretical model in which an H_2 molecule is located above a graphene surface. The present model of graphene consists of 37 C and 15 H atoms, in which C atoms at edges of graphene are passivated by H atoms. As shown in Fig. 1(b), some atoms emphasized as C1, H1, and H2 are featured due to steric conformations of the C and H atoms considered to be effective for the dissociative adsorption of H_2 above grpahene surfaces. It is known that H atoms mainly interacts with C atoms at the on-top site [Jeloacia and Sidis (1999); Sha and Jackson (2001)]. In this study, a graphene layer is modeled by $C_{37}H_{15}$, not by a coronene-like model ($C_{24}H_{12}$). Using this model, the system becomes symmetric around a centrally located C atom and the effect of edges can be reduced. On the other hand, by the use of coronene-like model, the symmetric structure cannot be maintained and the second-neighbor C atoms are located at the edges. It is expected that reactions of an H_2 molecule can be evaluated more accurately above the present model than above coronene-like models. A coupling procedure of *ab initio* methods and MD computations is applied to the dissociative adsorption process of an H_2 molecule above a graphene layer. This is one of the

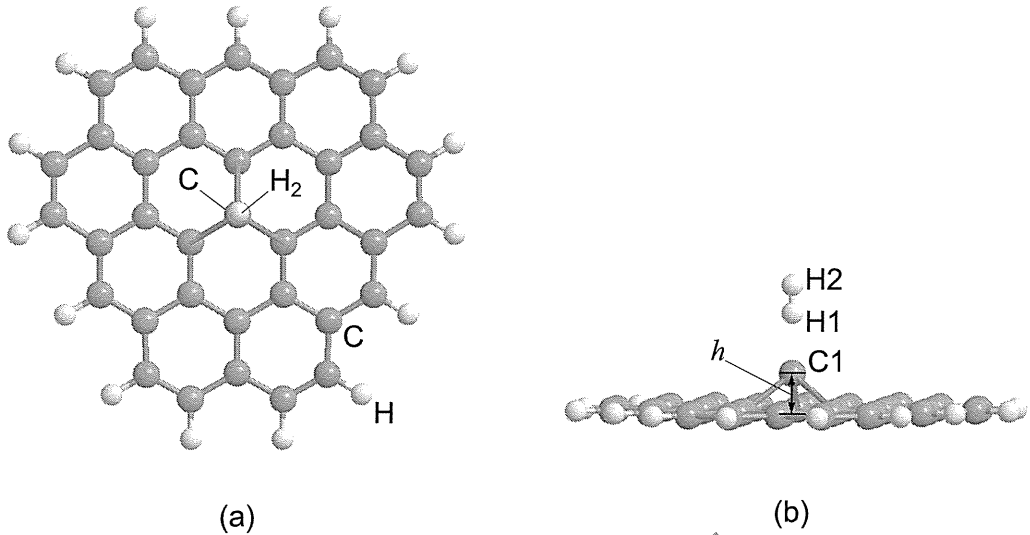

Figure 1: Schematic illustrations of computational models in which an H_2 molecule is located above a model graphene surface of $C_{37}H_{15}$: (a) top view of the system and (b) side view of distorted graphene in which the central C1 atom is elevated at a height h; the H_2 molecule consists of H1 and H2.

most effective procedures for investigating reaction dynamics induced by electron transfers between activated atoms.

The Hartree–Fock (HF) approximation which requires wave function convergences is employed to the *ab initio* MD simulations. It is important to consider the behavior of wave functions with a high accuracy when reactions are dominated by charge transfer. Furthermore, polyatomic molecular systems have many degrees of freedom and it is difficult to elucidate the reaction pathways fully by static energetical analyses. Therefore, we perform a dynamic analysis on the reaction system using an *ab initio* MD method in which the Lagrangian of the system is written as [Leforestier (1978); Deumens, Diz, Longo, and Öhrn (1994)]:

$$L\left(\{\mathbf{R}_i\},\{\dot{\mathbf{R}}_i\}\right)=\sum_i^N \frac{1}{2}M_i\dot{\mathbf{R}}_i^2-E_{\mathrm{HF}}\left(\{\mathbf{R}_i\},\{\psi_k\}\right), \tag{1}$$

where $\mathbf{R}_i$ and $\dot{\mathbf{R}}_i$ respectively denote the position and velocity of the ith nucleus, M_i the nuclear mass, and ψ_k an electron wave function of the kth eigenstate. Each electron is quantized and settles in discrete eigenstates. The electronic contributions are calculated in the framework of HF approximation. The potential energy E_{HF} includes nuclear repulsions, nucleus–electron and electron–electron interactions. From Eq. (1), the equation of motion of the ith nucleus is derived

as $M_i\ddot{\mathbf{R}}_i = -\partial E_{\mathrm{HF}}/\partial \mathbf{R}_i$. Considering quantum mechanical contributions to atomic motions, the gradient of E_{HF} is calculated based on the Hellmann–Feynman theorem [Feynman (1939)]. The Hamiltonian of a system is derived from Eq. (1) and is given by [Leforestier (1978); Deumens, Diz, Longo, and Öhrn (1994)]

$$H(\{\mathbf{R}_i\},\{\mathbf{P}_i\}) = \sum_{i=1}^{N} \frac{\mathbf{P}_i^2}{2M_i} + E_{\mathrm{HF}}(\{\mathbf{R}_i\},\{\psi_k\}), \tag{2}$$

where $\mathbf{P}_i$ is the momentum of the ith nucleus. The Hamiltonian is conserved during the computation, *i.e.*, $\dot{H} = 0$. Electrons that contribute to atomic forces are always in the ground state and never break the adiabatic approximation. The unrestricted HF method is employed for open-shell structures such as $C_{37}H_{15}$ and $C_{37}H_{15}$+H_2. Electronic structures are obtained using the GAUSSIAN 03 computational code [Frisch et al. (2004)]. Electrons in a function space are expanded in terms of a linear combination of atomic orbitals. Pople's 3–21G(d,p) basis set is employed for the present simulations and 6–31G(d,p) basis set is used for potential energy analyses. For the validation of *ab initio* MD simulation, the normal vibration of H_2 is evaluated by Fourier analysis for the periodic vibration. As a result, a spectrum of normal vibration mode can be obtained and its value corresponds to 53.53 kJ/mol. The experimetal value is known to be 50.96 kJ/mol [Witmer (1926)]. The computational result slightly overestimates the experimental data but have a considerable agreement with it. The other well-known techniques in the procedures were reported in previous studies [Kawano (1998); Doi, Haga, Shintaku, and Kawano (2010)]. Integrals of the equation of motion are performed using the velocity Verlet algorithm [Allen and Tildesley (1989)]. The simulation time step is set to 0.5 fs. A time step should be chosen properly for efficient electronic structure computations and for maintaining the conservation laws, although excessively short time steps will prevent long period simulations. The present value of time step is confirmed to conserve the total Hamiltonian of the present system well. The criteria of energy convergence are set to 2.62×10^{-7} kJ/mol. In the *ab initio* MD computations, errors in the total energy are estimated as 0.2 % for 1 ps simulations. Temperature is assumed to be 0 K at initial conditions. Therefore, momentum distributions and thermal effects are not considered in the present simulations. A main purpose is to demonstrate an advantage of this method to find out reaction pathways efficiently. Although computational results strongly depend on the initial configurations, a continuous reaction of dissociative adsorption of H_2 can be clarified by this method and additional potential surface analyses. However, the evaluation of free energies depending on temperature and other experimental conditions is our future work.

3 Results and Discussion

3.1 *Preliminary study on ab initio MD*

Before discussing the *ab initio* MD results, we present a fundamental analysis from the viewpoints of both quantum mechanical and classical mechanical approaches. Figure 2 shows potential energy curves depending on the interactions between an H atom and a planar graphene surface. Here, H1 is located above an on-top site of C1 which is located at the center of graphene, as shown in Fig. 1. A difference in atomic interactions which cause different pictures between *ab initio* MD and classical MD simulations is described later. In Fig. 2, the abscissa is a distance between C1 and H1. The potential energy curves obtained with and without quantum mechanical considerations exhibit quite different characteristics. A curve which was obtained by considering quantum effects had an energetically stable point at 1.15 Å and the dissociation energy of H atom from the graphene was 96.0 kJ/mol. This value is in reasonable agreement with the previous work [Sha and Jackson (2001)]. However, the dissociation limit of the interaction does not converge due to a constraint of the HF approximation. Our main purpose is to perform faster *ab initio* MD computations to search for chemical reaction pathways which are enhanced by charge transfer. More accurate analyses on the electronic structures for the dissociation limits are beyond the scope of this study. On the other hand, without quantum mechanical considerations, H1 which approaches the graphene surface experiences weak attractive forces and it will find a physically stable point near the surface. The dissociation energy of this interaction was evaluated as 1.78 kJ/mol at a distance of 3.05 Å. This weak interaction is caused by the intermolecular force and is well fitted by the following Lennard–Jones type potential:

$$V(r) = 31.3\left[\left(\frac{2.61}{r}\right)^7 - \left(\frac{2.61}{r}\right)^6\right]. \tag{3}$$

In this case, the attractive interaction of C1–H1 bond is proportional to $1/r^6$ and it is dominated by the van der Waals interaction. Note that a difference between the curves in Fig. 2 is caused by the different descriptions of electronic motions. In the classical mechanical framework, the atomic force is derived from the gradient of electrostatic potentials of ions, where the electronic distributions do not directly contribute to the interactions. In contrast, in the quantum mechanical approach, electronic distributions vary with the transformation of molecular structures, since the behavior of electrons is explicitly treated on the basis of electrostatic interactions. Figure 2 clearly reveals that the strong C1–H1 bond is caused by electron transfers.

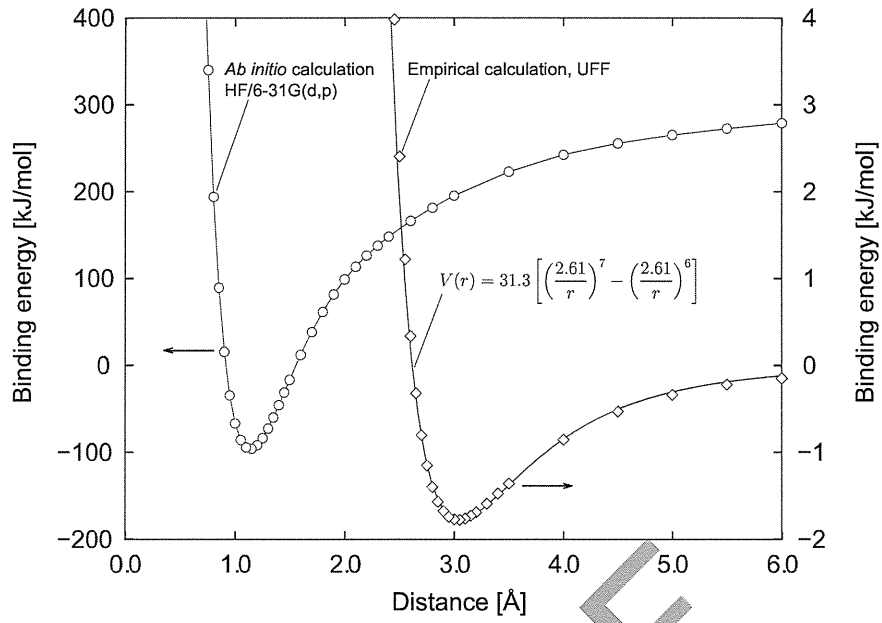

Figure 2: Potential energy curves of an H atom above the central C atom in a graphene layer of $C_{37}H_{15}$ calculated using *ab initio* methods by HF approximation, empirical methods using universal force field (UFF), and Lennard-Jones type potenial.

3.2 Ab initio MD results for dissociative adsorption of H_2

In this section, results of *ab initio* MD simulations for dissociative adsorption of H_2 above a graphene surface are discussed. Table 1 shows the computational results for different initial conditions. The initial conditions given in Tab. 1 are prepared for twelve cases of **a**–**l** from infinite number of conditions. In the present computations, initial momenta of the system are set to zero, since this study gives the first step to clarify the nature of phenomenon. Therefore, the results appear to be affected by the initial molecular structures. The possibility of H_2 adsorption on planar and steric graphene surfaces was investigated. In the case of steric surface, C1 which was centrally located in the graphene was elevated above the plane by a height h, as shown in Fig. 1(b). The height h was set to 1.0 Å to enhance H_2 dissociative adsorption. The molecular axis of H_2 was perpendicular or parallel to the surface. The bond lengths of H_2 were set to 0.75 and 1.20 Å for representing an equilibrium structure and an excessively stretched structure, respectively. For both the planar and the steric surfaces, the center of mass of an H_2 molecule was located at 2.0 Å above C1 in the case of **a**–**h**, and H1 was located at 2.0 Å directly above C1 in the case of **i**–**l**. In the case of **e**–**l** in which an H_2 molecular axis was parallel

to the grapnene surface, the H1–H2 axis was located above one of C1–C axses. As a result, adsorption of an H atom due to H_2 dissociation was observed only in the case of **d**. Neither dissociation nor adsorption were observed in the other cases: **a**–**c** and **e**–**l**. The present results indicate that several conditions have to be satisfied simultaneously to induce the dissociative adsorption of H_2 as shown in the case of **d**. In particular, the H1–H2 bond should be stretched excessively and be near to the graphene surface; the molecular axis of H_2 should be perpendicular to the surface; a steric configuration of C atoms is required to create the adsorption sites. In addition, the present results suggest that parallel conformations of H_2 to the graphene surfaces are not suitable for promoting dissociative adsorption of H_2. However, these limited results could elucidate only a few cases in all possibilities. Therefore, more details about other conformations and other conditions should be investigated in our continuous works. Hereafter, discussions are concentrated on the cases **a**–**d** in which an H1–H2 axis is perpendicular to the graphene surfaces to elucidate the nature of the phenomenon in detail.

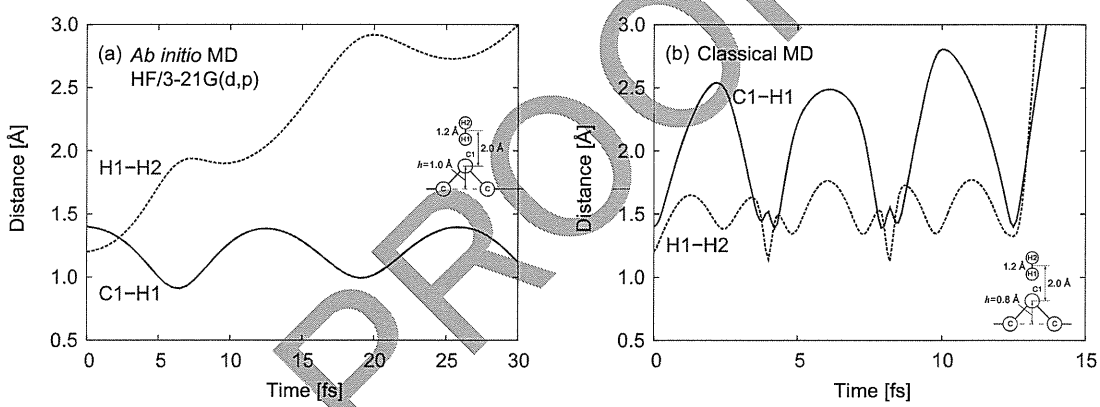

Figure 3: Transitions in the C1–H1 bond length (solid line) and dissociated H1–H2 length (dashed line) obtained using (a) *ab initio* MD with HF/3-21G(d,p) method for initial condition **d** and (b) classical MD for inital condition **d** with substitution of elevated height $h = 0.8$ Å of C1.

Figure 3 shows transitions of H1–H2 and C1–H1 lengths which promote the dissociative asdorption of H_2. This result was obtained using the initial condition of **d**. As shown in Fig. 3(a), the C1–H1 length oscillates periodically and the H2 atom leaves the graphene layer as time progresses. In this case, the H_2 molecule seems to be activated sufficiently to break H1–H2 bond at the initial condition and to promote adsorption of H1 to C1. A reaction pathway will be clarified by the potential energy surface analysis later. For comparison, a classical MD simulation was carried out under the similar conditions as the *ab initio* MD simulations. In

this case, the height h of C1 was initially set to 0.8 Å from the surface and the H_2 molecule was in the same condition as **d**. When C1 was located at 1.0 Å above the surface (i.e., the same value as for condition **d** in Tab. 1), the graphene layer became too unstable to maintain the structure (this figure is omitted). This instability is mainly caused by the different potential functions used in the *ab initio* MD and in the classical MD. In the present classical MD, the universal force field (UFF) [Rappé, Casewit, Colwell, Goddard III, and Skiff (1992)] was employed for atomic interactions. Consequently, the H_2 molecule bounces above C1 and neither H nor H_2 adsorb on the graphene surface, as shown in Fig. 3(b). Therefore, the dissociative adsorption of H_2 on graphene surfaces should be simulated using advanced MD methods coupling with quantum chemical methods. However, other methods in which the effect of electron transfer is considered empirically have been developed and their progresses are expected to treat chemical reaction systems efficiently [Warshel and Weiss (1980); Schmitt and Voth (1998)]. The results shown in Fig. 3 reveal a drastic difference between the *ab initio* MD and the classical MD calculations. Therefore, the *ab initio* MD method which considers time-dependent electronic motions is very effective to investigate the elementary process of dissociative adsorption of molecules, even though it constrains a short time step and consumes a long computational time.

Figures 4–6 show sequential snapshots of computational results for the conditions of **b**, **c**, and **d**, respectively. In the case of **b** as shown in Fig. 4, above the planar graphene surface, an H_2 molecule dissociated from the surface. At the initial condition of $t = 0$ s, the distance of H1–H2 was set to 1.20 Å and that of C1–H1 to 1.40 Å. Regardless of the excessively stretched H1–H2 bond, the H_2 and the graphene repulsively interacted with each other. In the case of **a**, the result showed similar tendency with that of **b**. Therefore, the details about **a** are omitted here. Figure 5 shows the behavior of H_2 on the steric graphene surface corresponding to the case **c**. In this case, at the initial condition, C1 was elevated at 1.0 Å from the planar surface; the length of H1–H2 was set to 0.75 Å; the distance between C1 and H1 was 1.63 Å. As time progressed, C1 appeared to be attracted by the graphene which maintained the planar structure. On the other hand, the H_2 molecule repulsively dissociated from the surface. In addition, its bond length of 0.75 Å was almost the optimized length and then the vibration between H1 and H2 was little activated. Figure 6 shows the result of condition **d** in which the dissociative adsorption of H_2 was successfully observed. In this case, an excessively stretched H_2 molecule was located above the steric graphene surface. As shown in Fig. 6(b) at $t = 10$ fs, the H1–H2 bond was cleaved due to the attractive interaction between H1 and C1. After that, H1 adsorbed on the graphene as C1 was pulled to the graphene layer. On the other hand, H2 dissociated from H1 and C1 repulsively. These results

Table 1: Twelve samples of initial conditions and results of *ab initio* MD computations.

Table 1

Type	Configulation*	Structure	h [Å]	H1–H2 length [Å]	C1–H1 length [Å]	Result
a	perpendicular	planar	0.0	0.75	1.63	Not adsorbed
b	perpendicular	planar	0.0	1.20	1.40	Not adsorbed
c	perpendicular	steric**	1.0	0.75	1.63	Not adsorbed
d	perpendicular	steric**	1.0	1.20	1.40	Adsorbed
e	parallel†	planar	0.0	0.75	2.00	Not adsorbed
f	parallel†	planar	0.0	1.20	2.00	Not adsorbed
g	parallel†	steric**	1.0	0.75	2.00	Not adsorbed
h	parallel†	steric**	1.0	1.20	2.00	Not adsorbed
i	parallel‡	planar	0.0	0.75	2.00	Not adsorbed
j	parallel‡	planar	0.0	1.20	2.00	Not adsorbed
k	parallel‡	steric**	1.0	0.75	2.00	Not adsorbed
l	parallel‡	steric**	1.0	1.20	2.00	Not adsorbed

* H1–H2 axis is perpendicular or parallel to the grapehene surface.

** C1 is elevated from the planar graphene surface.

† The center of mass of H_2 is directly above C1 and H1–H2 axis is located above one of C1–C axes.

‡ H1 is on-top site of C1 and H1–H2 axis is located above one of C1–C axes.

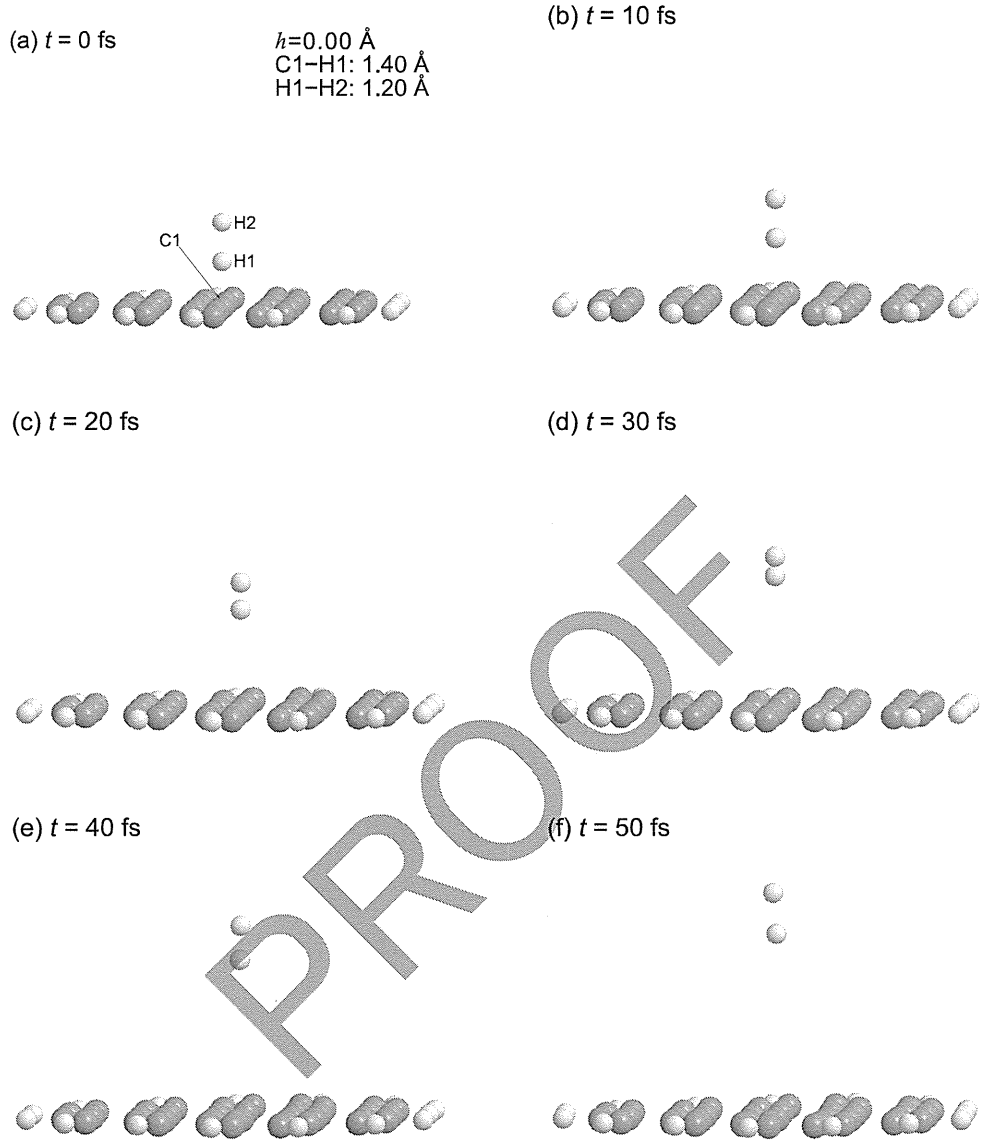

Figure 4: Snapshots of *ab initio* MD simulation with HF/3-21G(d,p) level for initial condition **b** in which h is 0.00 Å, C1–H1 length is 1.40 Å, and H1–H2 length is 1.20 Å: (a) 0 s, (b) 10 fs, (c) 20 fs, (d) 30 fs, (e) 40 fs, and (f) 50 fs.

mentioned above can be analyzed quantitatively in terms of the Mulliken atomic charge and the bond lengths. Figure 7(a) shows the transitions of C1–H1 and H1–H2 lengths and of Mulliken charges of C1, H1, and H2, in the case of **b**. It is clarified that the H_2 molecule those vibration is excited leaves from the graphene. C1 negatively charged at the initial state turns to be positive as the H_2 molecule

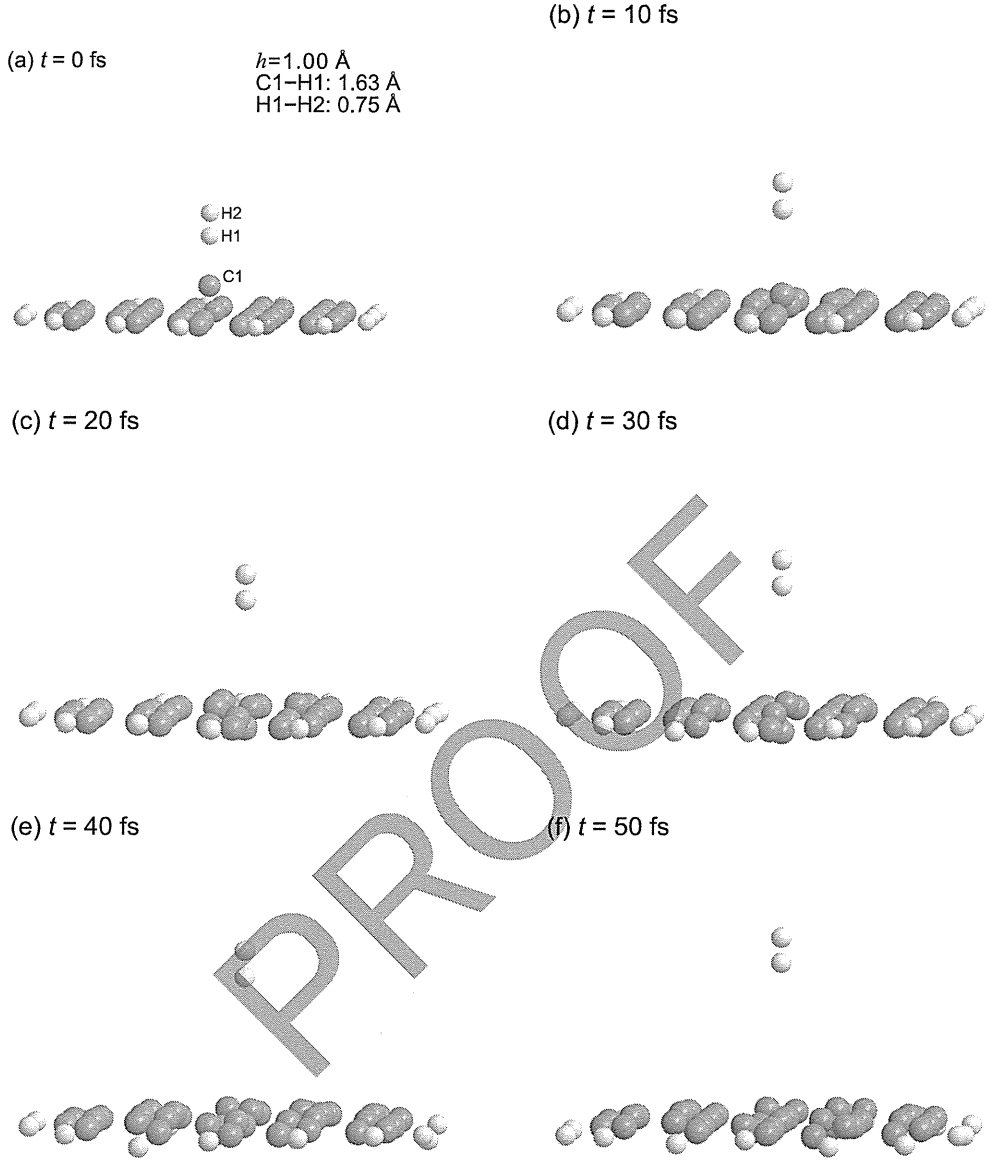

Figure 5: Snapshots of *ab initio* MD simulation with HF/3-21G(d,p) level for initial condition **c** in which *h* is 1.00 Å, C1–H1 length is 1.63 Å, and H1–H2 length is 0.75 Å: (a) 0 s, (b) 10 fs, (c) 20 fs, (d) 30 fs, (e) 40 fs, and (f) 50 fs.

dissociates from the surface. On the other hand, positive charges on H1 decrease as time progresses. The H_2 molecule and the graphene appear to be polarized to stabilize their electronic state at the initial condition. However, the charges begin to transfer through those atoms in order to make the system more stable as soon as the system is released. As time progressed, the polarization between C1, H1,

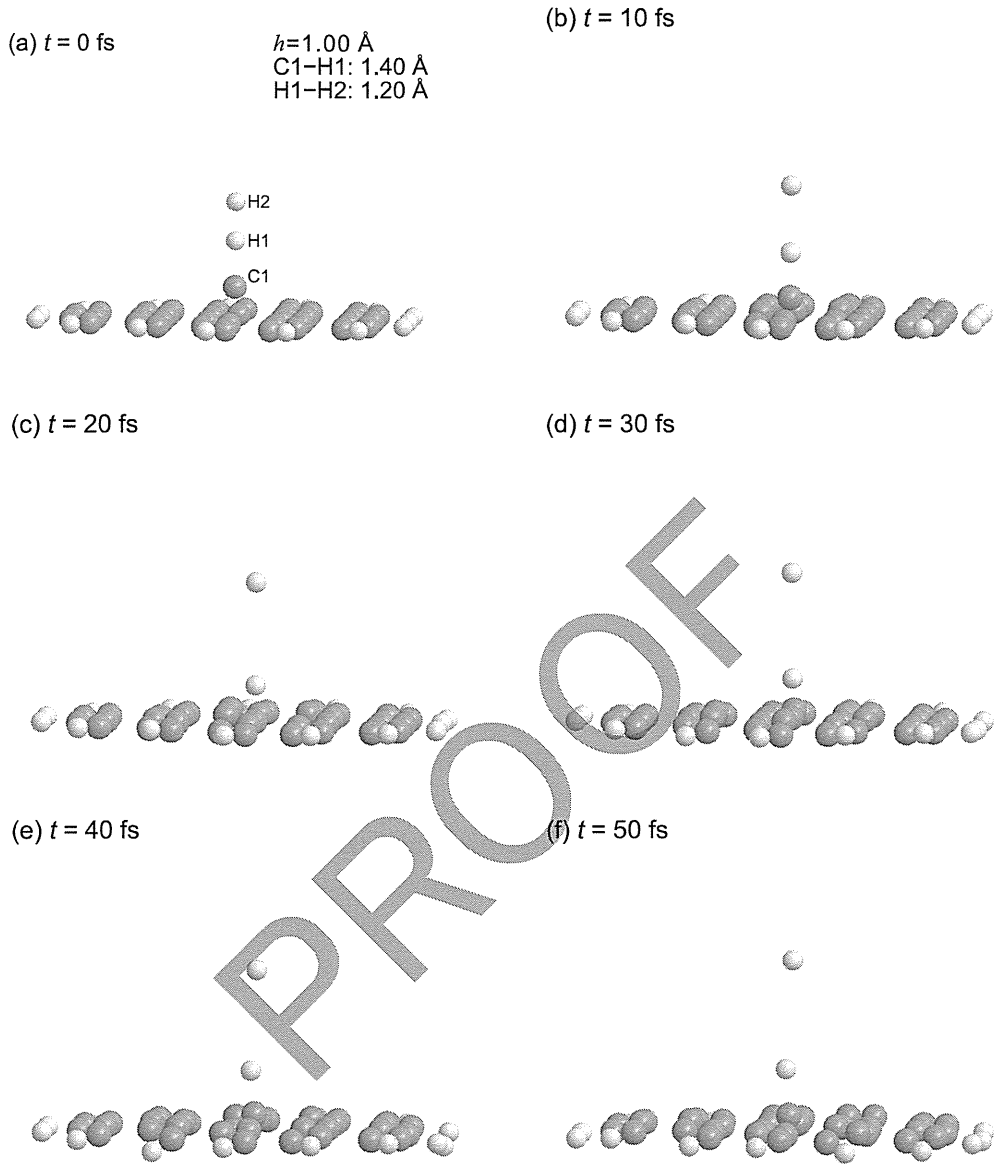

Figure 6: Snapshots of *ab initio* MD simulation with HF/3-21G(d,p) level for initial condition **d** in which h is 1.00 Å, C1–H1 length is 1.40 Å, and H1–H2 length is 1.20 Å: (a) 0 s, (b) 10 fs, (c) 20 fs, (d) 30 fs, (e) 40 fs, and (f) 50 fs.

and H2 tends to be depolarized. Therefore, chemical reactions such as dissociative adsorptions of H_2 cannot be expected in this system. Figure 7(b) shows the result of case **c** in which the H_2 molecule is almost optimized. Therefore, the charge transfer through H1 and H2 is little. The distance between C1 and H1 increases monotonically, regardless of the behavior of C1 which is affected by the nearby C

atoms. The charge transfer between C1 and H_2 is not so remarkable that chemical reactions cannot be observed. On the other hand, in the case of **d** as shown in Fig. 7(c), different characteristics from those in Figs. 7(a) and 7(b) can be obtained due to charge transfer which induces the chemical reaction. In this case, C1 and H1 are polarized at the initial condition, although H2 is almost neutral. As time progresses, H1 becomes more positive and the periods of charge transfer between C1 and H1 appear to synchronize with each other according to the stretching vibration of C1–H1. The period can be roughly estimated to be 11 fs and the length of C1–H1 is averagely maintained at 1.20 Å. In particular, the maximum and minimum points of atomic charge of adsorbed H1 approximately coincide with the peak points of C1–H1 length. This result implies that electrons move from the graphene to the adsorbed H1 atom as the C1–H1 length stretches and that the Mulliken charge shows peaks at the points where the C1–H1 bond length is maximized. Time-averaged values for the atomic charge are 0.231 and −0.282 for H1 and C1, respectively. Generating the C1–H1 bond, H2 turns to be neutral and separates from H1 and C1. It is found that the H1–H2 bond is cleaved slowly different from the separation of H_2 from the graphene surface as shown in Figs. 7(a) and 7(b). These results indicate that the charge transfer correlates with molecular vibrations and that these electrons play an important role in the intramolecular interactions. On the other hand, the intermolecular dynamics which are not affected by charge transfer and chemical reactions can be described in the framework of conventional MD methods [Kawano (1998); Doi, Haga, Shintaku, and Kawano (2010); Allen and Tildesley (1989)]. The present result in Fig. 7(c) successfully demonstrates a typical characteristic of chemical reactions enhanced by charge transfer.

Figure 8 shows sequential snapshots of a molecular orbital observed in the initial stage of dissociative adsorption of an H_2 molecule for the condition **d**. Isosurfaces of the electron wave function are presented in addition to the atomic positions. Electronic elementary steps in the early period can be discussed from this figure. In the initial condition as shown in Fig. 8(a), an electron is separately observed on the H_2 molecule and the graphene surface. As shown in Figs. 8(b)–8(d), the electronic distribution on the H_2 molecule transfers to the graphene side as the H_2 approaches C1 of the graphene. The behavior of charge transfer which synchronizes with the periodic vibration of C1–H1 bond is observed in the first 10 fs. Figures 7(c) and 8 reveal charge transfer which generates repulsive force between H1 and H2 and then the repulsive interaction triggers the dissociation of H1–H2 bond. On the other hand, a chemical bond is formed between the H1 and C1 atoms due to the transferred electrons and due to the polarization between them. Depending on the distance between H1 and C1, the electronic distribution is stabilized instantaneously and apears to be synchronized with the vibration. This is an overview of